Tip-Enhanced Second Harmonic Generation From a Single $NaNbO_3$ Nanocrystal

Gengxu Chen, E. Wu, Chengjie Ding, Quanlan Xiao, Xueting Ci, Yan Liu, Youying Rong, Botao Wu, Jianrong Qiu, and Heping Zeng

***Abstract*—We demonstrated the enhanced second harmonic generation (SHG) from a single sodium niobate ($NaNbO_3$) nanocrystal by approaching a metal tip on top of it. By scanning a laser-focused $NaNbO_3$ nanocrystal with a gold-coated tip, the mapping of the enhanced SHG from the nanocrystal was obtained. We observed that the SHG of the single $NaNbO_3$ nanocrystal was strongly enhanced with the gold-coated tip on the top of it. And the enhancement factor showed strong dependence on the excitation polarization and the excitation power. An over 12-fold tip enhancement was observed when the excitation power was 12 mW.**

***Index Terms*—Second harmonic generation (SHG), single sodium niobate ($NaNbO_3$) nanocrystal, tip enhancement, polarization dependence, power dependence.**

I. Introduction

SECOND harmonic generation (SHG) microscopy, based on nonlinear process, is recently considered as an promising technique for the applications in biolabeling [1]–[4], bioimaging [5]–[7], inorganic material characterization [8]–[10] and so on at the submicrometric scale or even nanoscale. Compared to the two-photon excitation fluorescence that loses energy during the relaxation of the excited states, the SHG photons have exactly half the wavelength of the incident light entering the nonlinear χ^2 media, which is an energy-conserving two-photon process. Nanoscale optical nonlinear properties of different materials such as $KTiOPO_4$ and $Fe(IO_3)_3$ have been recently investigated [11], [12]. They show perfect photostability and non-blinking behavior, which are the key properties for the SHG microscopy applications like long-term cellular imaging [13]. Compared to a fluorescent-based biolabel, there's no photobleaching or saturation effect on the emission rate of second-harmonic photons for the reason that the nonlinear interaction doesn't involve excited state populations [7]. The SHG intensity from the nonlinear nanocrystals is technically only limited by the damage threshold of the hosting environment.

Manuscript received September 29, 2014; revised December 31, 2014; accepted March 10, 2015.

G. Chen, E. Wu, C. Ding, X. Ci, Y. Liu, Y. Rong, B. Wu, and H. Zeng are with the State Key Laboratory of Precision Spectroscopy, East China Normal University, Shanghai 200062, China (e-mail: hiu.gxchen@gmail.com; ewu@phy.ecnu.edu.cn; dcjnonno@163.com; 842219415@qq.com; 541927011@qq.com; 1693314718@qq.com; btwu@phy.ecnu.edu.cn; hpzeng@phy.ecnu.edu.cn).

Q. Xiao and J. Qiu are with the State Key Laboratory of Luminescent Materials and Devices, Institute of Optical Communication Materials, South China University of Technology, Guangzhou 510640, China (e-mail: xiaoquanlan@126.com; qjr@scut.edu.cn).

Color versions of one or more of the figures in this paper are available online at http://ieeexplore.ieee.org.

Digital Object Identifier 10.1109/JSTQE.2015.2413406

Generally, strong electromagnetic field is required for nonlinear optical process due to the fact that the high order polarization tensor is much smaller than the first order. Fortunately, plasmonic effect can lead to strong localized electromagnetic fields by coupling to incident light, resulting in higher effective nonlinearities of the metal itself or the surrounding dielectric material [14]–[20]. Metallic nano/micro materials and structures are usually designed and used for producing the plasmonic effects. Among all of them, the metal tip is outstandingly noted for enhancing the photoluminescence or the Raman signals [21]–[25]. A highly localized electromagnetic field can be generated at the metal tip because of the plasmonic oscillation. Therefore, the strengthened field at the tip boosts the excitation rate that corresponds to an enhanced excitation density provided by the light source, which improves the effective optical response in the nonlinear process.

In this paper, we demonstrated tip-enhanced SHG from a single nonlinear optical nanocrystal of sodium niobate ($NaNbO_3$), which would be a potential technique for imaging based on SHG microscopy and tip enhancement effect. By investigating the optical properties of the tip-enhanced SHG from the $NaNbO_3$ nanocrystal, we observed that the tip enhancement factor exhibited strong dependence on the excitation fundamental wave polarization and power. In addition, there existed plasmonic enhancement effect on both the fundamental wave and the SHG, which interplayed delicatly resulting in the total tip-enhancement. But the dominant one was changing dependent on the excitation power. An over 12-fold enhancment was obtained at the excitation power of 12 mW.

II. Experimental Setup

$NaNbO_3$, which is environmentally friendly, is regarded as a promising lead-free piezoelectric and photocatalytic material [26], [27]. In addition, as a nonlinear optical material [28], it is currently attracting much interest in both scientific and engineering. The $NaNbO_3$ nanocrystals in this work were produced by a two-step hydrothermal method [29]–[31]. Firstly, $KNbO_3$ nanoparticles were prepared by hydrothermal method. As the raw materials for the next step, the $KNbO_3$ nanoparticles were added with NaOH aqueous solution. Then the hydrothermal method was applied again to the solution. Finally, the $NaNbO_3$ nanoparticles were obtained. Fig. 1(a) shows X-ray diffraction (XRD) patterns of the synthesized $NaNbO_3$ nanocrystal samples. From Fig. 1(a), it can be observed that all diffraction peaks are assigned as a pure cubic phase structure (JCPDS No. 75–2102, space group: $Pm-3m$, $a=b=c=0.3906$ nm). And it was also proved by the corresponding scanning electron

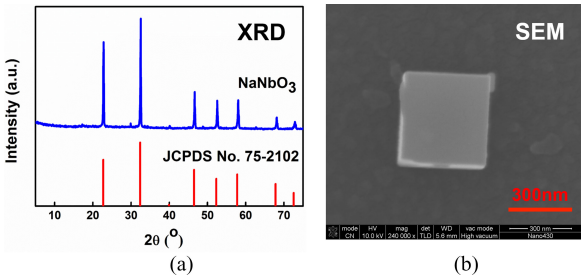

Fig. 1. (a) XRD patterns of the synthesized $NaNbO_3$ nanocrystals, indicating a cubic phase structure (JCPDS No. 75-2102). (b) SEM image of a typical single $NaNbO_3$ nanocrystal, which showed obviously a cubic structure. Scale bar is 300 nm.

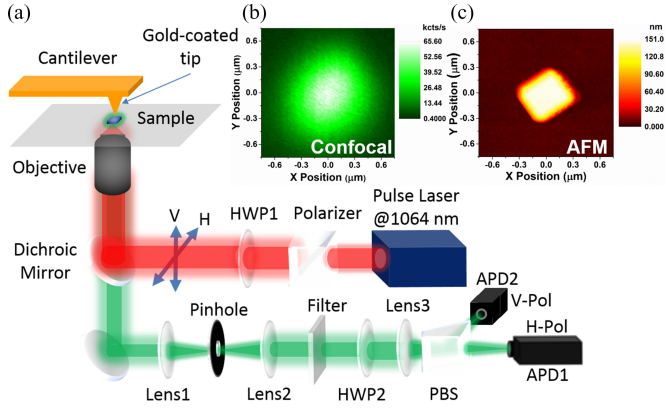

Fig. 2. (a) Experimental schematic for tip-enhanced SHG from $NaNbO_3$ nanocrystals. HWP1, halfwave plate at 1064 nm; HWP2: half wave plate at 532 nm; PBS, polarization beamsplitter; APD1/2, single photon detectors based on Si-APDs for horizontal polarization (H-Pol) and vertical polarization (V-Pol), respectively. (b) SHG image of a single $NaNbO_3$ crystal acquired with the scanning confocal microscope. The laser scan area is $1.5 \times 1.5\ \mu m^2$. (b) Topographic image of the same single $NaNbO_3$ crystal obtained by the AFM. The AFM tip scan area is $1.5 \times 1.5\ \mu m^2$.

microscope (SEM) image. As shown in the SEM image in Fig. 1(b), the size of the cubic $NaNbO_3$ nanocrystal was about few hundreds of nanometers.

For cubic phase $NaNbO_3$, its structure exhibits a complicated three-dimensional (3D) network composed of NbO_6 distorted polyhedra. The Nb-$O_{1(2,3,4,5,6)}$ distances of 1.9530Å are all the same in a NbO_6 octahedron with a symmetrical center, then further interconnecting into a 3D framework [32, Fig. 2]. The bandgap of the $NaNbO_3$ is 3.25 eV. And the $NaNbO_3$ crystal is transparent in the visible and infrared regime [33]. For nonlinear optical applications, it initially appears irrational to use cubic phase $NaNbO_3$ due to its centrosymmetric crystal structure. SHG activity is strictly forbidden by symmetry. However, the SHG of the cubic phase $NaNbO_3$ nanocrystals is still observed. The inversion symmetry may be broken at the surface of the nanocrystals [34], which arouse the SHG in the cubic phase $NaNbO_3$. Therefore, the nonlinear optical response of the cubic phase $NaNbO_3$ nanocrystal could be described by a nonlinear source polarization:

$$\overrightarrow{P}^{(2)}(2\omega) = \varepsilon_0 \overleftrightarrow{\chi}_s^{(2)} L(2\omega)L(\omega)L(\omega) : \overrightarrow{E}(\omega)\overrightarrow{E}(\omega) \qquad (1)$$

where $\overleftrightarrow{\chi}_s^{(2)}$ denotes the surface nonlinear susceptibility tensor with the components $\overleftrightarrow{\chi}_{s,\perp\perp\perp}^{(2)}$, $\overleftrightarrow{\chi}_{s,\perp\parallel\parallel}^{(2)}$, $\overleftrightarrow{\chi}_{s,\parallel\perp\parallel}^{(2)}$. $L(\omega)$ and $L(2\omega)$ are the local-field correction factors for the pump and generated optical fields $\overrightarrow{E}(\omega)$ and $\overrightarrow{E}(2\omega)$, respectively [35].

After the synthesis procedure, the $NaNbO_3$ nanocrystals were dispersed in ethanol (99.7% purity) with a concentration of about 0.25 mg/ml. In order to homogenize the solution, we put it in the ultrasonic bath for 10 min. 50 μL of the solution was dropped on a clean coverslip with roughness of 1–2 nm for spin coating. Then we got a sample with an average distribution density of $NaNbO_3$ about $0.01/\mu m^2$ on the coverslip.

We studied the SHG of $NaNbO_3$ nanocrystals by a combined system of a scanning confocal microscope and an atomic force microscope (AFM). As illustrated schematically in Fig. 2(a), a home-built Yb-doped pulsed fiber laser emitting at 1064 nm with a repetition rate of 30 MHz and a pulse duration of 11 ps was used as the excitation source. After a polarizer at the output of the fiber laser, the excitation laser became a linear polarized one. And with a half-wave plate following the polarizer, the polarization angle could be easily varied. Then the laser beam was focused on the coverslip by an oil-immersion objective ($\times$100, N.A. = 1.40, oil immersion, UPlanSApo, Olympus). The beam size at the focus was about 1 μm. The resultant SHG from the single $NaNbO_3$ nanocrystals was collected by the same microscope objective. The SHG signal was filtered spectrally by a dichroic mirror and a band-pass filter at 532 nm with bandwidth of 3 nm. And the beam was also spatially filtered by a pinhole with diameter of 75 μm in a telescope system. The SHG signals were finally detected by single-photon detectors based on Si-avalanche photondiodes (APDs). In order to analyze the polarization property of the SHG from the $NaNbO_3$ crystals, a half-wave plate at 532 nm (HWP2) together with a polarization beamsplitter was set in front of the two orthogonal-aligned APDs. The polarization state of the SHG could be checked by continuously tuning HWP2. The sample of the coverslip with $NaNbO_3$ nanocrystals was held on an *x*-*y* piezo stage. By scanning the piezo stage, the confocal image of the single $NaNbO_3$ nanocrystal was obtained as shown in Fig. 2(b).

On the top of the scanning confocal microscope, an AFM (NanoWizard II, JPK) was installed to acquire the surface topograph of the nanocrystal. The tip used here for plasmonic enhancement is made of silicon with a gold coating layer of 70-nm thickness (SI-AF01-A, SEIKO). It is shaped into a pyramid structure of 12.5 μm height with a curvature radius of 30 nm on the tip. The tip of the AFM was aligned coaxially with the confocal microscope. Fig. 2(c) shows the topographic image of the same single $NaNbO_3$ nanocrystal in Fig. 2(b). The shape of the $NaNbO_3$ nanocrystal was a cubic of about 550 nm (long) $\times$ 500 nm (short) $\times$ 150 nm (high), in good agreement with the SEM image.

And a spectrograph could be switched on to replace the single-photon detectors to acquire the spectrum of the SHG photons. Fig. 3 shows the spectrum of the SHG spectrum from the single $NaNbO_3$ nanocrystal with excitation laser at 1064 nm as shown in the inset of Fig. 3. The SHG wavelength was at 532 nm, exactly half of the wavelength of the fundamental wave.

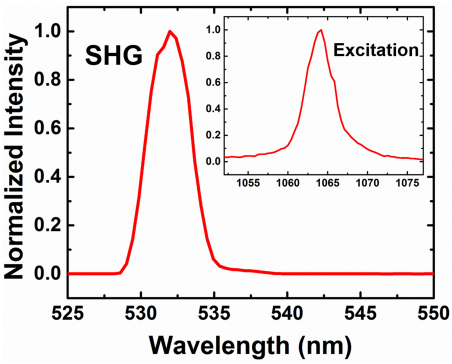

Fig. 3. Spectrum of the SHG from the single cubic $NaNbO_3$ nanocrystal. Inset: Excitation laser spectrum.

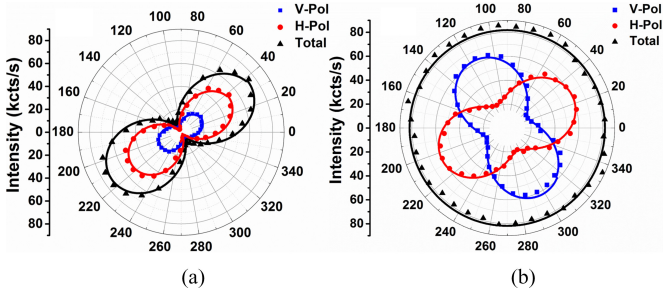

Fig. 4. Polarization dependence of the SHG from $NaNbO_3$ crystal. (a) SHG intensity (black triangles) and its vertical polarization component (blue rectangles), horizontal polarization component (red spots) as a function of the excitation polarization angle with their sine fits. (b) Total SHG intensity (black triangles) and its polarization property at excitation polarization angle of 35°.

III. Results and Discussions

Due to the possible SHG signal from the gold-coated tip itself [35], we firstly checked the SHG response of the tip by removing the sample while scanning the tip at the laser focus area. However, there was no distinguishable SHG response observed. Considering the axial excitation and collinear axial detection in our case, it was in agreement with results in the Ref. [35].

Besides, in order to verify if the tip was damaged, we acquired a separate AFM image for each measured laser power illumination, and check whether it was still same as that without excitation. For avoiding the damage of the tip, we limited the laser power to below 12 mW.

There exist symmetry selection rules for SHG scattering for nanostructure. With different selection of excitation direction and polarization, the polarizations of the SHG reveal diverse contributions in various detection direction [35]. Thus it is necessary to investigate the polarization properties of the SHG signal.

Without the effect of the AFM tip, the polarization properties of the SHG signal were recorded as a reference. The excitation laser was kept at 10 mW. In order to investigate the effect of the excitation polarization on the SHG, the HWP1 was tuned while monitoring the SHG intensity on the two APDs. We defined the vertical polarization as 0°, corresponding to the *X*-axis in the confocal and AFM images in Fig. 2(b) and (c). The SHG intensity on horizontal and vertical polarization components together with the total intensity as functions of the excitation polarization were recorded and shown in Fig. 4(a). With rotation of the excitation polarization angle, the total intensity of the SHG changed periodically. And the maximum or minimum SHG intensities of the orthogonal polarization components were acquired in the same excitation polarization, indicating that the polarization angle of the SHG photons did not change with the excitation polarization angle. The maximum SHG was obtained when the excitation polarization angle was about 35°, which was along the long edge of the nanocrystal cubic.

While fixing the excitation polarization angle at 35° to obtain the maximum SHG signal, we tuned the HWP2 for analyzing the polarization state of the SHG from the $NaNbO_3$ crystal. And polarization angle was about 125°, which was orthogonal to the excitation laser polarization, indicating a type I phase matching

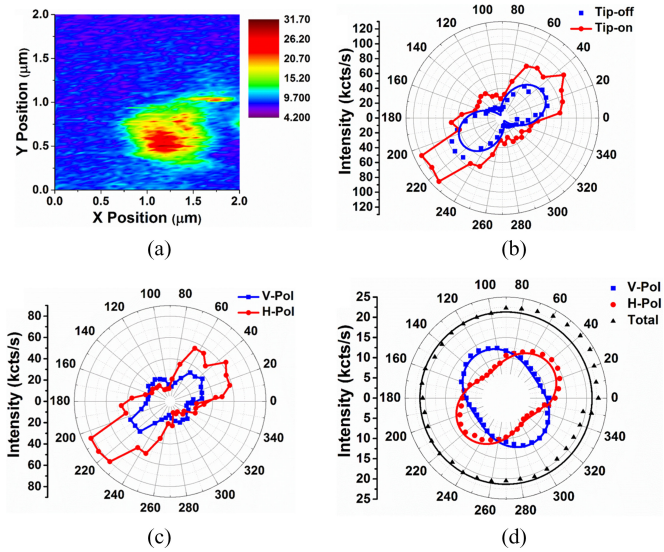

Fig. 5. Tip-enhanced SHG from $NaNbO_3$ crystal. (a) A mapping image of the SHG intensity dependent on the position of the gold tip. The AFM tip was scanning line by line along the long edge of the $NaNbO_3$ nanocrystal cubic. The scan area is $1.5 \times 1.5\ \mu m^2$. (b) Enhanced SHG intensity (red spots) as a function of the excitation polarization angle with comparison of non-enhancement (blue rectangles). (c) Vertical polarization component (blue rectangles) and horizontal polarization component (red spots) of SHG intensity as a function of the excitation polarization angle. (d) Enhanced SHG polarization property at excitation polarization angle of 125°.

SHG process (o + o→e) was taking place in the nanocrystal. The polarization contrast was about 0.535 by fitting the polarization intensity with a sine-wave function.

In order to investigate the tip-enhancement of the SHG, the gold-coated tip approached to the top of the nanocrystal while the laser was focused on the center of the nanocrystal. Since the size of the laser beam at the focus was much larger than the nanocrystal, the whole nanocrystal was within the illumination of the laser while the AFM tip was scanning the surface. We monitored the SHG intensities on the two APDs. Then we obtained the mapping of the SHG intensity dependent on the position of the AFM tip as presented in Fig. 5(a). The AFM tip was scanning line by line along the long edge of the $NaNbO_3$ nanocrystal cubic. As the gold-coated tip was close to

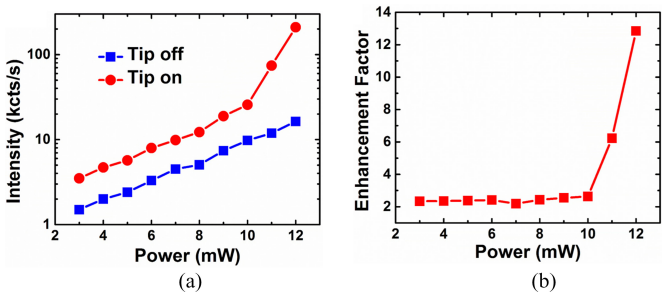

Fig. 6. (a) Enhanced SHG intensity (red spots) as a function of the excitation power with comparison of non-enhancement (blue rectangles). (b) Enhancement factor as a function of the excitation power.

the laser-focused area, the field enhancement was chiefly confined to the vicinity of the gold-coated tip apex as a result, and it rapidly decayed as the distance between the tip and the laser-focused area. The tip-enhanced SHG mapping reproduced the topographic image of the nanocrystal in Fig. 2(c). The SHG mapping appeared bigger than the AFM image because the height of the $NaNbO_3$ nanocrystal was larger than the curvature radius of the gold-coated tip and when the pyramid side of the tip approached the vertical side of the nanocrystal cubic, SHG intensity was also enhanced, leading to a stretching of the image.

The influences of the excitation polarization on the SHG enhancement were presented in Fig. 5(b). The excitation laser power was still kept at 10 mW for comparison. With the AFM tip on the nanocrystal, the SHG intensities were much enhanced at all excitation polarization angles. But the enhancement factor was not the same. When the excitation polarization was at about 125°, meaning along the short edge of the nanocrystal cubic, we observed the maximum enhancement factor of 3.18 when the gold-coated tip approached to the nanocrystal. Without the tip, the intensity of the SHG was only 11 kcounts/s. With the tip approached, the SHG intensity increased to 35 kcounts/s. Fig. 5(c) shows the polarization components variation with the excitation polarization. Different from the SHG without enhancement, when the excitation polarization was at 125°, the vertical polarization component of the SHG was not the minimum. Instead, it was much enhanced and contributed to the maximum enhancement factor, indicating that the enhancement factor was not unique for different polarization components, which would be caused by the asymmetric structure of the pyramid-shaped AFM tip. As shown Fig. 5(d), the polarization angle of the tip-enhanced SHG intensity maintained almost the same as that without the enhancement. However, the polarization contrast decreased to 0.303. The decrease of the polarization contrast also verified the different enhancement factors in different polarization angles.

Furthermore, the power dependence of the enhancement factor was investigated as well. Keeping the excitation polarization at 125°, we varied the excitation power. As shown in Fig. 6(a), without the tip-enhancement, the SHG signal increased quadratic with the excitation power with a slope of 0.115 in linear-logarithmic diagram, exhibiting the feature of the second-order nonlinear process. With the tip-enhancement, the SHG signal increased with the excitation power. When the excitation power was below 10 mW, the slope was 0.121, which was almost same as that without the tip, indicating that the plasmonic resonance was taking place directly with the electromagnetic field of SHG more strongly than with the incident field of the fundamental wave, leading to an independence of the enhancement factor with a value of about 2.4 on excitation power as presented in Fig. 6(b). However, when the excitation power was beyond 10 mW, the slope rapidly increased to 0.456. It revealed that the plasmonic enhancement of the electromagnetic field of the fundamental wave overwhelmed that of the SHG field when the excitation power was beyond 10 mW, resulting in a rapidly increased enhancement factor with the excitation power as depicted in. Fig. 6(b). When the excitation power reached 12 mW, an over 12-fold enhancement on the SHG was observed. It should be noted that in the measurement with 12 mW excitation, the AFM image was the same as that at low excitation power, ensuring the tip was not damaged. Larger enhancement on the SHG intensity would be expected with further increase on the excitation power. However, the damage threshold of the gold-coated tip and the nanocrystals should be taken into consideration.

IV. Conclusion

In conclusion, we demonstrated the enhanced SHG from a single sodium niobate ($NaNbO_3$) nanocrystal by approaching a metal tip on top of it. The enhanced SHG originated from the enhancement of a highly localized electromagnetic field in the vicinity of the metal tip induced by plasmonic effect. We observed that the enhancement factor showed strong dependence on the excitation polarization and the excitation power. An over 12-fold tip enhancement was observed when the excitation power was 12 mW. Taking advantages of photostability and no saturation effect appearing from the nonlinear process, tip-enhanced SHG microscopy would be a promising technique for applications in biolabelling and bioimaging with strongly enhancing signals in a localized area by a nanoscale metal tip.

References

[1] P. Pantazis, J. Maloney, D. Wu, and S. E. Fraser, "Second harmonic generating (SHG) nanoprobes for in vivo imaging," in *Proc. Nat. Acad. Sci.*, Jul. 2010, vol. 107, no. 33, pp. 14535–14540.

[2] N. Olivier *et al.* "Cell lineage reconstruction of early zebrafish embryos using label-free nonlinear microscopy," *Science*, vol. 329, no. 5994, pp. 967–971, Aug. 2010.

[3] D. Staedler *et al.* "Harmonic nanocrystals for biolabeling: A survey of optical properties and biocompatibility," *ACS Nano*, vol. 6, no. 3, pp. 2542–2549, Feb. 2012.

[4] L. Mayer *et al.* "Single KTP nanocrystals as second-harmonic generation biolabels in cortical neurons," *Nanoscale*, vol. 5, no. 18, pp. 8466–8471, May 2013.

[5] P. J. Campagnola, M. Wei, A. Lewis, and L. M. Loew, "High-resolution nonlinear imaging of live cells by second harmonic generation," *Biophys. J.*, vol. 77, pp. 3341–3349, Dec. 1999.

[6] L. Moreaux, O. Sandrea, and J. Mertz, "Membrane imaging by second harmonic generation microscopy," *J. Opt. Soc. Amer. B*, vol. 17, no. 10, pp. 1685–1694, Oct. 2000.

[7] P. J. Campagnola and L. M. Loew, "Second-harmonic imaging microscopy for visualizing biomolecular arrays in cells, tissues and organisms," *Nature Biotechnol.*, vol. 21, no. 11, pp. 1356–1360, Oct. 2003.

[8] S. Brasselet and J. Zyss, "Nonlinear polarimetry of molecular crystals down to the nanoscale," *Comptes Rendus Phys.*, vol. 8, no. 2, pp. 165–179, Mar. 2007.

[9] N. Sandeau *et al.* "Defocused imaging of second harmonic generation from a single nanocrystal," *Opt. Exp.*, vol. 15, no. 24, pp. 16051–16060, Nov. 2007.
[10] A. U. Chowdhury *et al.* "Kinetic trapping of metastable amino acid polymorphs," *J. Amer. Chem. Soc.*, vol. 136, no. 6, pp. 2404–2412, Feb. 2014.
[11] L. Le Xuan *et al.* "Photostable second-harmonic generation from a single $KTiOPO_4$ nanocrystal for nonlinear microscopy," *Small*, vol. 4, no. 9, pp. 1332–1336, Sep. 2008.
[12] L. Bonacina *et al.* "Polar $Fe(IO_3)_3$ nanocrystals as local probes for nonlinear microscopy," *Appl. Phys. B*, vol. 87, no. 3, pp. 399–403, Mar. 2007.
[13] T. Magouroux *et al.* "High-speed tracking of murine cardiac stem cells by harmonic nanodoublers," *Small*, vol. 8, no. 17, pp. 2752–2756, Sep. 2012.
[14] Y. Chi, G. Chen, F. Jelezko, E Wu, and H. Zeng, "Enhanced photoluminescence of single-photon emitters in nanodiamonds on a gold film," *IEEE Photon. Technol. Lett.*, vol. 23, no. 6, pp. 374–376, Mar. 2011.
[15] E. Wu *et al.* "Spatial polarization sensitivity of single Au bowtie nanostructures," *J. Lumin.*, vol. 131, no. 9, pp. 1971–1974, Sep. 2011.
[16] B. Wu, K. Ueno, Y. Yokota, K. Sun, H. Zeng, and H. Misawa, "Enhancement of a two-photon-induced reaction in solution using light-harvesting gold nanodimer structures," *J. Phys. Chem. Lett.*, vol. 3, no. 11, pp. 1443–1447, May 2012.
[17] M. Song *et al.* "Polarization properties of surface plasmon enhanced photoluminescence from a single Ag nanowire," *Opt. Exp.*, vol. 20, no. 20, pp. 22290–22297, Sep. 2012.
[18] A. Joushaghani *et al.* "Sub-volt broadband hybrid plasmonic-vanadium dioxide switches," *Appl. Phys. Lett.*, vol. 102, no. 6, art. no. 061101, Feb. 2013.
[19] G. Chen *et al.* "Photoluminescence enhancement dependent on the orientations of single NV centers in nanodiamonds on a gold film," *IEEE J. Sel. Top. Quantum Electron.*, vol. 19, no. 3, art. no. 4602404, May 2013.
[20] M. Song *et al.* "Photoluminescence plasmonic enhancement of single quantum dots coupled to gold microplates," *J. Phys. Chem. C*, vol. 118, no. 16, pp. 8514–8520, Apr. 2014.
[21] T. Ichimura, N. Hayazawa, M. Hashimoto, Y. Inouye, and S. Kawata, "Tip-enhanced coherent anti-stokes Raman scattering for vibrational nanoimaging," *Phys. Rev. Lett.*, vol. 92, no. 22, p. 220801, Jun. 2004.
[22] F. M. Huang, F. Festy, and D. Richards, "Tip-enhanced fluorescence imaging of quantum dots," *Appl. Phys. Lett.*, vol. 87, no. 18, p. 183101, Oct. 2005.
[23] E. Bailo and V. Deckert, "Tip-enhanced Raman scattering," *Chem. Soc. Rev.*, vol. 37, no. 5, pp. 921–930, Mar. 2008.
[24] Y. Y. Hui *et al.* "Tip-enhanced sub-diffraction fluorescence imaging of nitrogen-vacancy centers in nanodiamonds," *App. Phys. Lett.*, vol. 102, no. 1, p. 013102, Jan. 2013.
[25] R. Zhang *et al.* "Chemical mapping of a single molecule by plasmon-enhanced Raman scattering," *Nature*, vol. 498, no. 7452, pp. 82–86, Jun. 2013.
[26] G. Li, T. Kako, D. Wang, Z. Zou, and J. Ye, "Synthesis and enhanced photocatalytic activity of $NaNbO_3$ prepared by hydrothermal and polymerized complex methods," *J. Phys. Chem. Solids*, vol. 69, no. 10, pp. 2487–2491, Oct. 2008.
[27] H. Shi *et al.* "$NaNbO_3$ Nanostructures: Facile synthesis, characterization, and their photocatalytic properties," *Catal. Lett.*, vol. 132, no. 1, pp. 205–212, Sep. 2009.
[28] E. L. Falcao-Filho *et al.* "Third-order optical nonlinearity of a transparent glass ceramic containing sodium niobate nanocrystals," *Phys. Rev. B*, vol. 69, p. 134204, Apr. 2004.
[29] Z. Li, R. Liu, Y. Xie, S. Feng, and J. Wang, "A novel method for preparation of doped $Ba_3(Ca_{1.18}Nb_{1.82})O_{9-\delta}$: Application to ammonia synthesis at atmospheric pressure," *Solid State Ionics*, vol. 176, no. 11, pp. 1063–1066, Mar. 2005.
[30] M. Liu, D. Xue, and K. Li, "Soft-chemistry synthesis of $LiNbO_3$ crystallites," *J. Alloys Compounds*, vol. 449, no. 1, pp. 28–31, Jan. 2008.
[31] J. Wu and D. Xue, "Crystallization of $NaNbO_3$ microcubes by a solution-phase ion exchange route," *Cryst. Eng. Commun.*, vol. 13, no. 11, pp. 3773–3781, Apr. 2011.
[32] S. K. Mishra, N. Choudhury, S. L. Chaplot, P. S. R. Krishna, and R. Mittal, "Competing antiferroelectric and ferroelectric interactions in $NaNbO_3$: Neutron diffraction and theoretical studies," *Phys. Rev. B*, vol. 76, p. 024110, Jul. 2007.
[33] P. Li, S. Ouyang, Y. Zhang, T. Kako, and J. Ye, "Surface-coordination-induced selective synthesis of cubic and orthorhombic $NaNbO_3$ and their photocatalytic properties," *J. Mater. Chem. A*, vol. 1, no. 4, pp. 1185–1191, Jan. 2013.
[34] J. I. Dadap, J. Shan, and T. F. Heinz, "Theory of optical second-harmonic generation from a sphere of centrosymmetric material: Small-particle limit," *J. Opt. Soc. Amer. B*, vol. 21, no. 7, pp. 1328–1347, Jul. 2004.
[35] C. Neacsu, G. Reider, and M. Raschke, "Second-harmonic generation from nanoscopic metal tips: Symmetry selection rules for single asymmetric nanostructures," *Phys. Rev. B*, vol. 71, no. 20, p. 201402, May 2005.

Gengxu Chen was born in Fujian Province, China, in 1988. He received the B.S. degree in East China Normal University, Shanghai, China, in 2010, where he is currently working toward the Ph.D. degree. His current research interests include single photon generation and nanoplamonics.

E. Wu was born in Shandong Province, China, in 1979. She received the Ph.D. degree in optics from East China Normal University, Shanghai, China, in 2007. Her current research interest includes single-photon manipulation.

Chengjie Ding was born in Shanghai, China, in 1991. She received the B.S. degree in East China Normal University, Shanghai, China, in 2013, where she is currently working toward the M.S. degree. Her current research interests include single photon generation and nanoplamonics.

Quanlan Xiao was born in Jiangxi Province, China, in 1986. She is currently working toward the Ph.D. degree at the South China University of Technology, Guangzhou, China. Her current research interest includes nanomaterials.

Xueting Ci was born in Shaanxi Province, China, in 1990. She received the B.S. degree in Xidian University, Xi'an, China, in 2012. She is currently working toward the M.S. degree in East China Normal University, Shanghai, China. Her current research interest includes surface plasmon of noble metal nanostructure.

Yan Liu was born in Shandong Province, China, in 1988. He received the B.S. degree in Yunnan University, Kunming, China, in 2011. He is currently working toward the Ph.D. degree in East China Normal University, Shanghai, China. His current research interest includes single photon generation.

Youying Rong was born in Shanxi Province, China, in 1991. She received the B.S. degree in Lanzhou University, Lanzhou, China, in 2014. She is currently working toward the M.S. degree in East China Normal University, Shanghai, China. Her current research interest includes single photon generation.

Botao Wu was born in Henan Province, China, in 1979. He received the Ph.D degree from the Shanghai Institute of Optics and Fine Mechanics, Chinese Academy of Science, Shanghai, China, in 2008. His research interest includes surface plasmon of noble metal nanostructure.

Jianrong Qiu was born in Zhejiang Province, China, on February 14, 1964. He received the Ph.D. degree from Okayama University, Okayama, Japan, in 1992. He joined Zhejiang University as a Qiu-Shi Professor in 2005, and joined the South China University of Technology as a Cheung-Kung Professor in 2009. His research interest includes luminescent materials and devices.

Heping Zeng was born in Hunan Province, China, on August 28, 1966. He received the B.S. degree in physics from Peking University, Beijing, China, in 1990, and the Ph.D. degree from the Shanghai Institute of Optics and Fine Mechanics, Chinese Academy of Science, Shanghai, China, in 1995. He joined East China Normal University as a Cheung-Kung Professor in 2000. His research interest includes ultrafast photonics and single-photon optics.